Characterization of Internalization and Endosome Formation of Epidermal Growth Factor in Transfected NIH-3T3 Cells by Computerized Image-intensified Three-dimensional Fluorescence Microscopy

M. Benveniste,* J. Schlessinger,‡ and Z. Kam*

* Department of Polymer Research and ‡ Department of Chemical Immunology, The Weizmann Institute of Science, Rehovot, 76 100, Israel

Abstract. Computerized image-intensified fluorescence microscopy has been used to quantify routing and subcellular concentrations of rhodaminated EGF (Rh-EGF) during its receptor-mediated endocytosis in two transfected NIH-3T3 cell lines expressing 2×10^5 and 1.5×10^6 receptors per cell, respectively. A series of images were digitized by focusing at different depths through the volume of a single cell. The digitized pictures were corrected for fluorescence photobleaching, and removal of out-of-focus fluorescence contributions by deconvolution using the point spread function of the microscope optics (Agard, D. A., and J. W. Sedat. 1980. *Proc. Soc. Photo-Opt. Instr. Eng.* 264:110–117) allowed automatic computer analysis of the time dependence of endosomal vesicle size and fluorescence intensity in a live cell and also enabled the study of isolated vesicles. An increase in the amount of fluorescence bound to the cell surface, either by increasing the number of receptors expressed per cell or the concentration of Rh-EGF in the incubation drop, yielded an increase in the total fluorescence of internalized vesicles without an increase in their number and area. The linear relation between fluorescence intensity and area for vesicles at different times indicates that EGF concentration is conserved. This is compatible with fusion of small vesicles to form larger ones. However, as endocytosis proceeds, a twofold increase in the slope of the fluorescence vs. area plots is observed for larger vesicles, suggesting that active sorting causes the EGF to be concentrated. Alternatively, this factor could be produced by cumulative fluorescence contributions from stacked membranes. Since coated pits are internalized independent of their occupancy with EGF receptor, we propose that endocytosis does not involve a mechanism specifically recognizing occupied receptors but is rather triggered by a global intracellular event.

EPIDERMAL Growth Factor (EGF) when bound to its receptor, causes a variety of cellular responses that eventually lead to proliferation (Carpenter and Cohen, 1979). Concomitant with these responses and associated biochemical changes in membrane and cytoplasmic proteins, both ligand and receptor are internalized by the pathway known as receptor-mediated endocytosis (Schlessinger et al., 1983; Willingham and Pastan, 1985; Hopkins, 1986).

Electron microscopic studies have shown that EGF receptors are diffusely distributed on the membrane surface. 3 min after exposure to EGF at 37°C, the EGF–receptor complex is found in coated pits, whereupon it is internalized and transferred through endosomes to the Golgi apparatus (Haigler et al., 1978; Willingham and Pastan, 1982). There are some indications that a fraction of the receptors are recycled back to the membrane (Beguinot et al., 1985; Honegger et al., 1987), while the EGF and the nonrecycled receptors are sent to lysosomes (Gorden et al., 1978).

In the cases of low density lipoprotein or transferrin receptors, endocytosis is the mechanism by which ligand is brought into the cell for internal use (Goldstein et al., 1979; Brown et al., 1983; Dautry-Varsat et al., 1983). The role of endocytosis for EGF function is not clear since EGF is degraded in the lysosomes (Carpenter and Cohen, 1976*a*; Gorden et al., 1978; Dickson et al., 1983). Since it takes 6–8 h of continuous incubation with EGF to commit a cell to proliferate (Carpenter and Cohen, 1976*b*), the EGF receptor or its degradation products (Das and Fox, 1978; Fox and Das, 1979) may accumulate in specific cytoplasmic compartments and trigger cellular responses. Alternatively, endocytosis may be a mechanism for removal of the tightly bound EGF–receptor complex from the cell surface, which may be necessary to allow for continuing sensitivity of the cell to extracellular EGF.

M. Benveniste's present address is Laboratory of Developmental Neurobiology, NICHD, Building 36, Room 2A21, National Institutes of Health, Bethesda, MD 20892. J. Schlessinger's present address is Rorer Biotechnology Inc., Research Laboratories, 680 Allendale Road, King of Prussia, PA 19046.

Site-directed mutagenesis has been used as a tool to study the relationship between the structure of the receptor and the different functions with which it is associated. Deletion mutants lacking the whole kinase domain of the EGF receptor are neither endocytosed nor do they induce cell proliferation (Livneh et al., 1986). An insertion at cytoplasmic residue 888, which shifts the reading frame of the rest of the receptor, destroyed kinase activity, endocytosis, and mitogenic activity, while an insertion at residue 708 destroyed kinase activity but did not arrest endocytosis and mitogenic activity (Livneh et al., 1986; Prywes et al., 1986). Until now, no mutant has been found that has mitogenic activity and does not undergo receptor-mediated endocytosis. This fact is indicative of the close relationship between the activation of endocytosis and mitogenicity. Since the latter involves a long sequence of unknown events, the study of endocytosis, the mechanism of its activation, and its relationship to the activation of other processes like phosphorylation and intracellular sorting is of interest.

Through the analysis of many fixed cells, electron microscopy has provided detailed information on receptor routing during endocytosis. Light microscopy can complement electron microscopy since one can follow the endocytic process throughout the whole cell over time and provide quantitative subcellular concentrations and distributions of fluorescently labeled probes within live cells. In addition to quantitative measurements with submicron spatial resolution, better temporal resolution of cellular responses can be obtained by observing an individual cell as compared with biochemical techniques which only give an averaged response of many unsynchronized cells.

Depending on the mechanism of trapping, internalization, and sorting of the EGF receptor, we can anticipate that controlled changes in ligand and receptor concentrations on the cell surface will differentially affect their concentrations in localized compartments and their distributions within the cell. Two NIH-3T3 cell lines (HER82 and HER22) which are devoid of endogenous murine EGF receptor, but were transfected with human EGF receptor cDNA, have been labeled with varying concentrations of rhodaminated EGF (Rh-EGF).[1] These lines express 1.5×10^6 and 2×10^5 receptors per cell on their surfaces, respectively (Benveniste et al., 1988). We have characterized the three-dimensional distribution of Rh-EGF by measuring fluorescence intensity as a function of time at a series of adjacent focal planes within the cell using computerized image-intensified microscopy. We have found that the concentration of EGF in endosomes was reduced by reducing the amount applied to the cells or by using cells with reduced expression of the EGF receptor. The number of endocytosed vesicles and their total membrane area varies less than twofold in all experiments with these two cell lines. The results suggest that the rate of endosome formation is almost independent of EGF and occupied receptor concentrations. We discuss these results in terms of possible activation mechanisms for endocytosis.

Materials and Methods

Cells

HER82 and HER22 are NIH-3T3 cell lines transfected with a full-length human cDNA construct of EGF receptor and have been described and characterized elsewhere (Benveniste et al., 1988). The cells were grown at 37°C and 5% CO_2 in DME containing 10% FCS and supplemented with 5 mM glutamine and combined antibiotics. Cells were grown on 18-mm^2 glass coverslips to 30% confluency in 35-mm tissue culture dishes. The coverslips were first treated for 1 h with 100 μg/ml poly-L-lysine hydrobromide (Biomakor, Jerusalem, Israel) followed by two washes with sterile water. 24 h after seeding, the cells were washed twice with 20 mM Hepes-buffered DME containing 10% FCS and lacking phenol red (HDME). The coverslips were then inverted onto parafilm containing a drop (usually 4 μl) of 5 or 50 μg/ml Rh-EGF (preparation described in Benveniste et al., 1988) and incubated for 5 min at room temperature. At this short time and with these high concentrations of EGF, one achieves a high level of binding that is proportional to concentration before considerable endocytosis occurs, avoiding incubation at low temperature as a means to arrest the process. Cells were washed twice and placed on a glass slide containing 6 μl of HDME. Experiments were then carried out at 37°C.

Image Collection

Fluorescently labeled cells were imaged using a microscope (Axiomat; Carl Zeiss, Inc., Oberkochen, FRG) equipped with a 100× 1.3-NA Planapo objective and epiluminescence (dichroic mirror with 510–560-nm excitation and 590-nm barrier filters) with a 100-W mercury lamp (Osram, Munich, FRG) and stabilized power supply (HBO 100 W/2; Carl Zeiss, Inc.). The incident light was attenuated by an iris inserted in the conjugated aperture plane. A second aperture in the incident beam-conjugated field plane limited the fluorescence excitation to the center of the microscope field where the image was digitized, thus reducing the background light level. The microscope zoom optics were used to further magnify the image twofold before it was projected onto a camera (ISIT; RCA, Lancaster, PA), digitized at 0.14 μm/pixel, or an image-intensified video camera (Venus TV2M; Carl Zeiss, Inc., Thornwood, NY), digitized at 0.17 μm/pixel by an image processor (FD5000; Gould de Anza Inc., San Jose, CA) interfaced with a computer (VAX 11/780; Digital Equipment Corp., Marlboro, MA). 32 video frames of 512 × 512 pixels were averaged in real time by the image processor, and a 256 × 256 eight-bit frame defined by a box cursor was transferred to the computer and stored for analysis. For each time point, eight focal planes were recorded by stepping the microscope focus at 2-μm intervals. Picture acquisition and storage, as well as the microscope focus and shutter, were controlled by the host computer using custom-made hardware (focus and shutter controller; Weizmann Institute of Science, Rehovot, Israel) and software (Felder, S., and Z. Kam, manuscript in preparation). Each such set of eight images defines a group with a total illumination time of 28 s. The time difference between groups varied progressively from 90 s, at the beginning of the collection, to 5 min.

Image Deconvolutions

Out-of-focus contributions were removed by using the adjacent planes three-dimensional deconvolution algorithm of Agard and Sedat (1980).

Calibration of Image Intensities

Since samples vary in fluorescence brightness, the camera controls the gain of its image intensifier to yield the optimal image. Calibration of the digitized grey levels was achieved by imaging a grey scale film consisting of six 15% OD steps transilluminated with a constant light source. When this grey scale was inserted into a conjugated field plane of the microscope, it was digitized simultaneously with each image, and the grey level values were stored with each picture. A least squares fitting program (Bevington, 1969) determines the slope and intercept that are used to calibrate the gain and blanking level of each picture and to normalize the digitized grey levels to those of one reference (a picture of an HER82 cell) used for all experiments. 0.5-μm-diameter rhodaminated polystyrene beads have been digitized at various gains and have demonstrated that there are no significant changes in the point spread function of our imaging system and that there are no distortions in our area estimations.

Bleach Correction

The intensity, I, for all pixels above a threshold, I_o, was summed for each group of eight focal planes and plotted as a function of the group number, n. These values were then used in a nonlinear least squares fitting program (Bevington, 1969) to determine the exponential decay constant of the fluorescence intensity due to bleaching, α. The bleach-corrected fluorescence, I_{mod}, for each pixel was then calculated according to

1. *Abbreviation used in this paper*: Rh-EGF, rhodaminated epidermal growth factor.

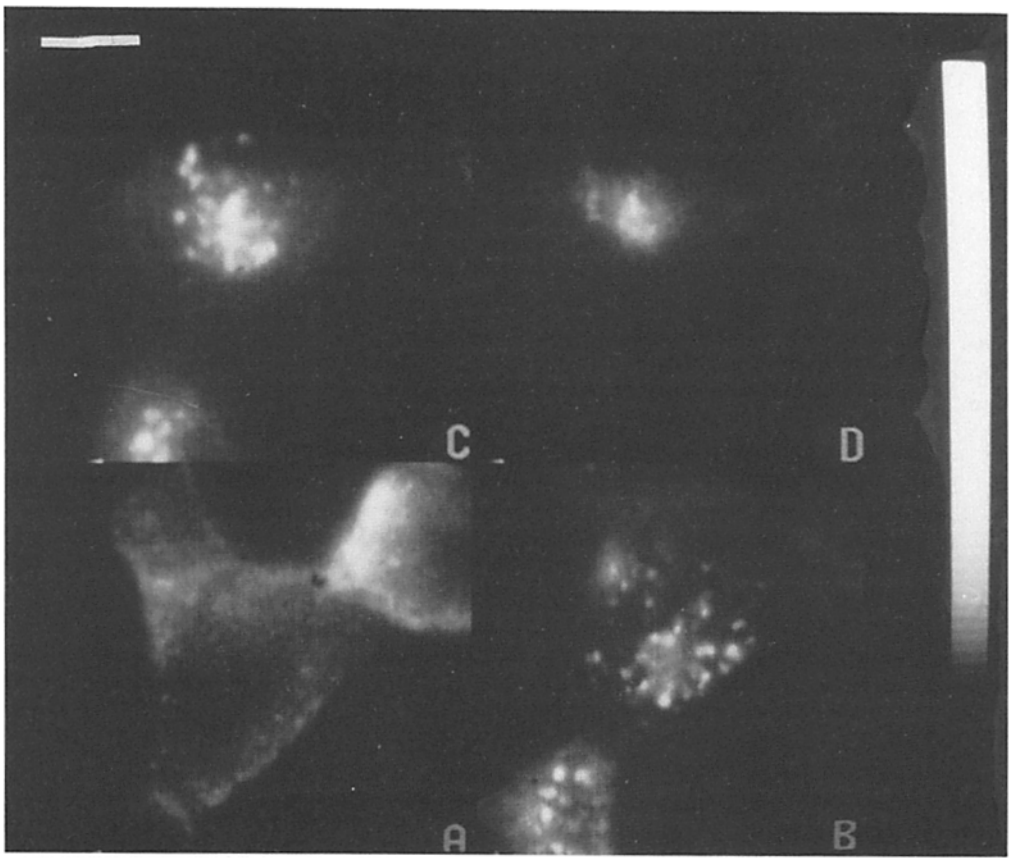

Figure 1. Progression of endocytosis of an HER82 cell labeled with Rh-EGF. The third focal plane (out of eight) is depicted at 0, 20, 40, and 60 min (*A–D*, respectively). The zero time under the microscope is ~10 min after the slide was incubated with Rh-EGF at room temperature. Bar, 5 μm.

$$I_{mod} = (I - I_o)\, e^{an} + I_o.$$

The threshold was defined as the grey level that gave the best segmentation between cell-associated fluorescence and out-of-cell background for the whole duration of the experiment. The main contributors to this background fluorescence were stray light scattered in the microscope and camera blanking level, which were constant for the duration of the experiment. Therefore, bleach corrections were not applied to values below the threshold.

Image Analysis

Endocytosis is quantified by first defining the regions inside the cell using manual mouse tracking of the inside boundary of the fluorescent membrane. The deconvoluted pictures are thresholded, and the areas within the mouse tracks are sorted into patches of contiguous pixels to give "vesicle area." This area represents a two-dimensional projection of the integrated intensity above the threshold collected from vesicles and is proportional to their cross-sectional area. Pixels belonging to the same patch were counted. Background-subtracted intensities from the corresponding areas of the original pictures were summed to yield the vesicle "fluorescence intensity." Only patches greater than or equal to two adjacent pixels (300 nm diameter) were used. The integrated intensities of all patches in the cell were plotted against the patch areas. The slope of the plot determined the "specific fluorescence."

Results

Fig. 1 shows the progression of endocytosis in an HER82 cell at various times after exposure to Rh-EGF. Fig. 1 *A* depicts the third focal plane of the cell, which is situated ~4 μm from the plane of attachment of the cell to the coverslip. The fluorescence observed by focusing through the focal planes is mostly membrane bound, although some small patches of fluorescence of 0.5 μm diameter are already visible adjacent to the plasma membrane inside the cell. The small degree of endocytosis observed is a result of incubating the cells with Rh-EGF at an endocytosis-permissive temperature of 22°C. The same focal plane of the same HER82 cell is imaged in Fig. 1 *B* after 20 min at 37°C. Larger fluorescent patches (1 μm diameter) have segregated toward the middle of the cell and the fluorescence appears mostly particulate. By comparing the plasma membranes in Fig. 1, *A* with *B*, a substantial decrease in fluorescence is observed. This exemplifies the decrease in diffuse fluorescence bound to the cell surface with the progression of endocytosis. Fig. 1 *C* depicts the same focal plane after a 40-min incubation. The cell has become rounded and most of the fluorescence has accumulated in the center and is no longer particulate in nature. 1 h after the start of the incubation at 37°C, the fluorescence intensity has completely concentrated in the center and no plasma membrane–associated fluorescence can be observed. A significant decrease in total fluorescence intensity between Fig. 1, *C* and *D*, is also apparent.

The incident light for all the experiments had to be kept approximately fivefold attenuated from the intensity of the source. If higher incident intensities were used, even briefly, endocytosis could not be observed. Yet, if cells were incubated with Rh-EGF for 10 min at 37°C to initiate endocytosis, the internalized fluorescent vesicles were observed to move and fuse, indicating that high intensities of the impinging light probably affect the early stages of endocytosis but may not affect later stages of intracellular routing.

The unprocessed images of these cells, which are 10–15 μm thick, contain significant out-of-focus fluorescence. By deconvoluting these images using the point spread function of the microscope, out-of-focus contributions are removed (Fig. 2). Segmentation of fluorescent endosomes from the background by a single threshold value for all the pictures imaged from one cell for the duration of the experiment is

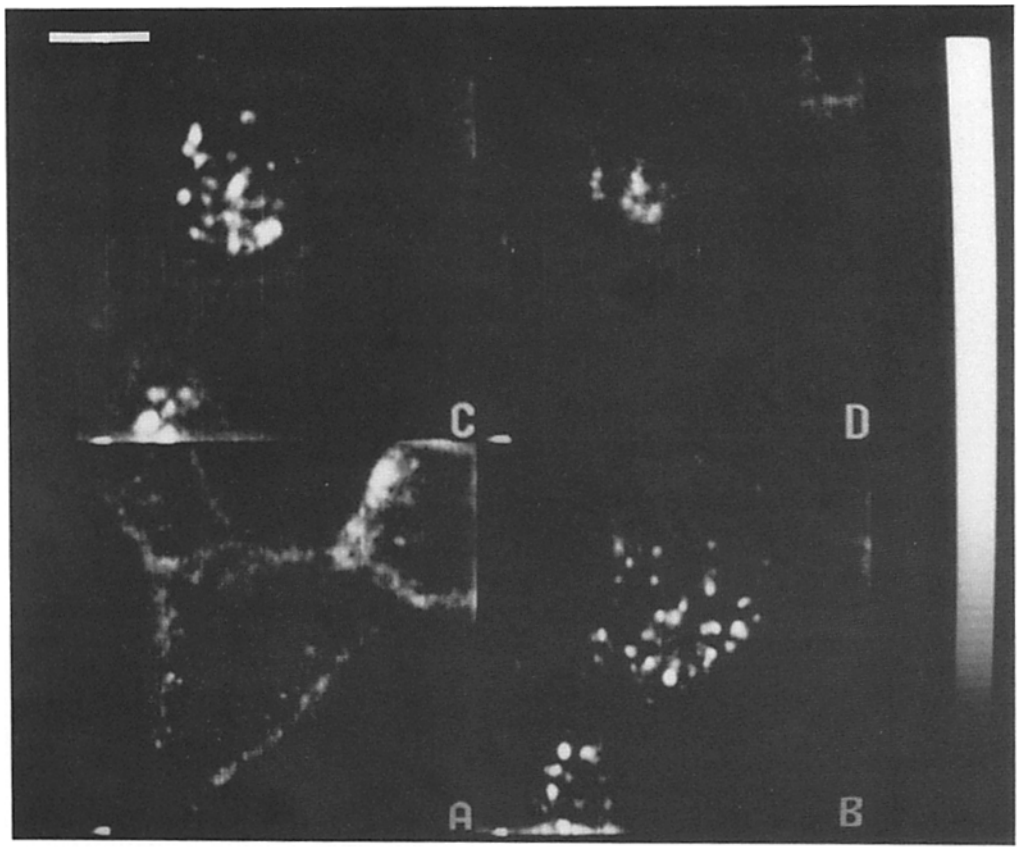

Figure 2. Same focal plane at times as in Fig. 1 after the three-dimensional deconvolution algorithm of Agard and Sedat (1980).

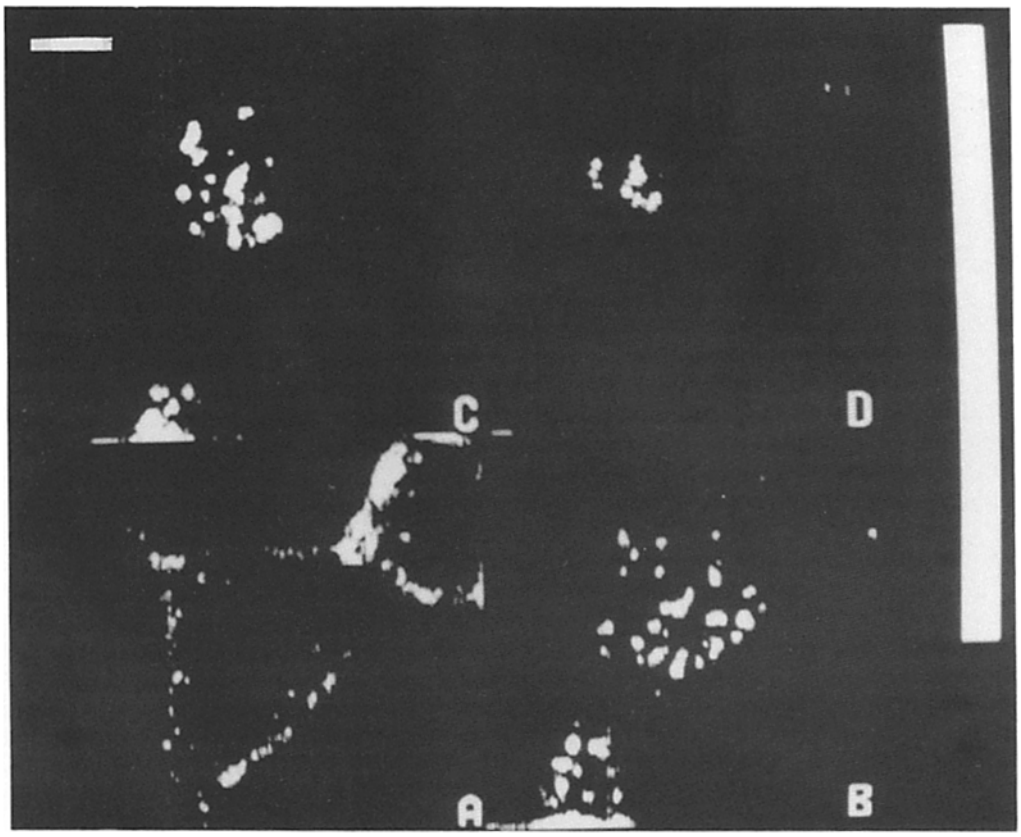

Figure 3. Thresholding of the deconvoluted optical sections of Fig. 2. The thresholded level is set interactively to provide the best segmentation of endosomes for all time groups of pictures of the same cell.

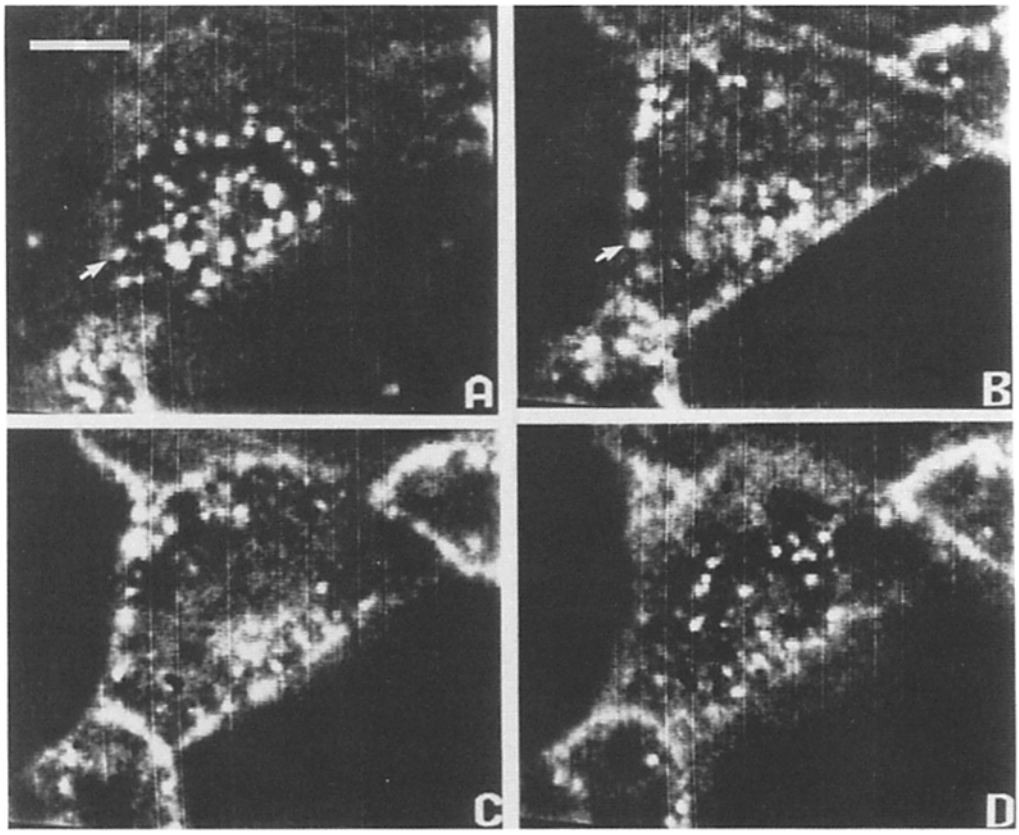

Figure 4. A set of consecutive optical sections of the cell depicted in Fig. 1, 10 min after the start of the experiment. Eight focal planes spanning the whole depth of the cell were deconvoluted. Four central deconvoluted optical sections from this set are shown. Most vesicles appear in only one section. Arrows depict the same large vesicle observed in two adjacent focal planes. Bar, 5 μm.

shown in Fig. 3. This process demonstrates that even in-focus diffuse fluorescence is easily kept below threshold. Fig. 4 displays four central deconvoluted optical sections (out of the total of eight collected at a time and spaced 2 μm apart) of the same HER82 cell as in Fig. 1, 10 min after the start of data collection (mid-time between Fig. 1, *A* and *B*). Most vesicles identified in one particular optical section are absent from adjacent sections. The high contrast between the vesicles and the surrounding background indicates that out-of-focus fluorescence contributions from the membrane and vesicles in other focal planes are insignificant. A few large vesicles are seen that contribute fluorescence in two consecutive image planes (Fig. 4, *A* and *B, arrows*). Fig. 5 shows the intensity profile of the vesicle indicated by the arrows in Fig. 4, *A* and *B*. The more distinct vesicle in Fig. 4 *B* corresponds to a sharper profile with an amplitude that exceeds the threshold of 70 used for this experiment, while the diffuse fluorescence of Fig. 4 *A* is far below the threshold level as shown in Fig. 5.

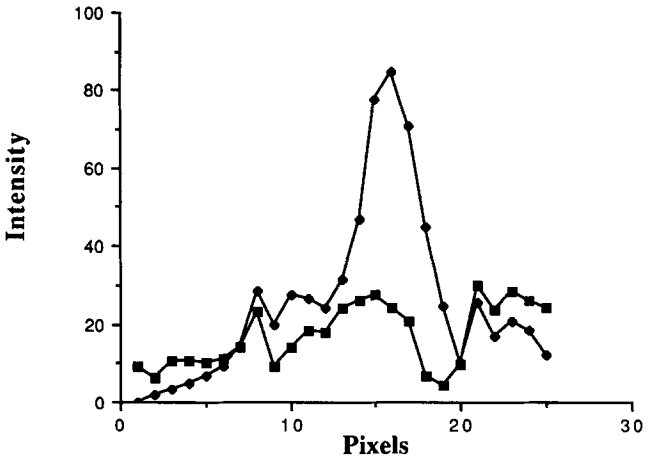

Figure 5. Intensity profile of a vesicle as it appears in two adjacent deconvoluted optical sections. (■) Intensity profile from a large vesicle pointed out by the arrow in Fig. 4 *A*; (♦) intensity profile from the same vesicle in Fig. 4 *B*.

Over the long time interval of these experiments, correct fluorescence intensities can be attained only after overcoming effects due to bleaching of the fluorophores and the consequent changes in the gain of the camera. Fig. 6 shows the normalized integrated cellular fluorescence of three representative cells: an HER82 cell incubated with 5 μg/ml Rh-EGF, an HER82 cell incubated with 50 μg/ml Rh-EGF, and an HER22 cell incubated with 50 μg/ml Rh-EGF. The fluorescence bleaching constant, α, of all three cells is similar and corresponds to an exposure time of 10 groups of images. Continuous illumination of HER82 cells for 14 min, equivalent to the accumulated intermittent exposures of 30 groups, yielded the same α. This is true for cells observed immediately after labeling with Rh-EGF as well as for cells incubated for 20 min at 37°C, which have internalized most of the Rh-EGF, and then illuminated for 14 min. The results of normalization for camera gain and bleach correction for integrated intensities of internalized fluorescence of an HER22 cell are shown in Fig. 7. The correction for camera gain, normalized to an HER82 cell, decreased the intensities approximately twofold. Bleach correction, which is time dependent, produces a curve of increasing internalized fluorescence, reaching a plateau after 30 min that is threefold higher than the original data.

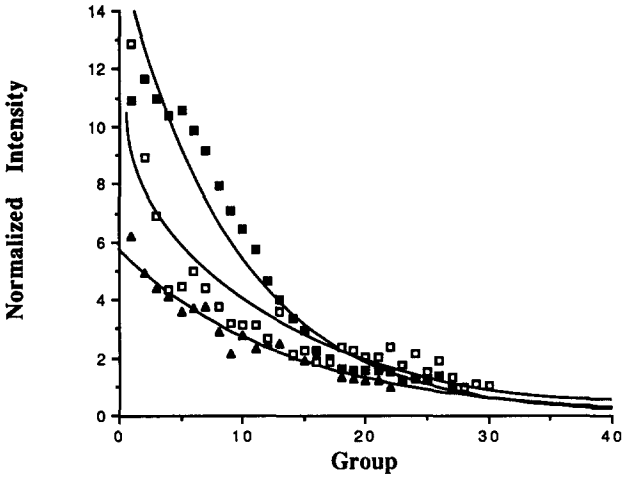

Figure 6. Fluorescent intensity decay due to bleaching. Integrated intensities of an HER82 cell labeled with 4 μl of 50 μg/ml Rh-EGF (■); an HER22 cell labeled with 4 μl of 50 μg/ml Rh-EGF (▲); and an HER82 cell labeled with 4 μl of 5 μg/ml Rh-EGF (□). Each curve consists of the summed image intensities above background of all eight focal planes as a function of time. These intensities were fitted to an exponential curve yielding the bleach decay constant, α, as described in Materials and Methods.

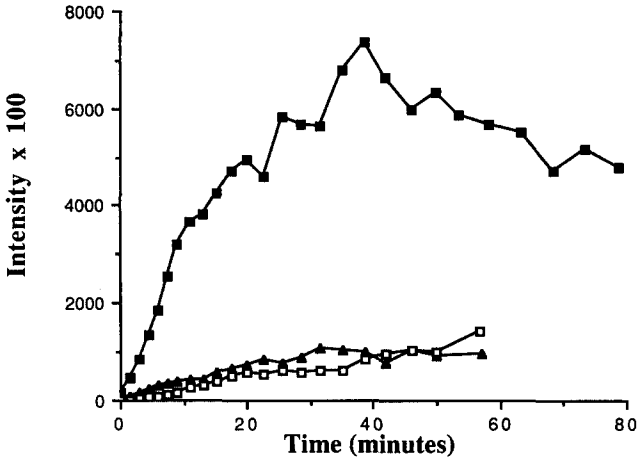

Figure 8. Time dependence of internalization of Rh-EGF by NIH-3T3 cells transfected with EGF receptor cDNA constructs. Integrated intensities (background subtracted) above threshold of each time group are summed and plotted for (■) HER82 cell labeled with 4 μl of 50 μg/ml Rh-EGF; (▲) HER22 cell labeled with 4 μl of 50 μg/ml Rh-EGF; and (□) HER82 cell labeled with 4 μl of 5 μg/ml Rh-EGF.

The time course for bleach-corrected and normalized internalized intensities for representative HER82 and HER22 cells is shown in Fig. 8. HER82 cells were incubated for 5 min on 4 μl of high EGF concentrations, either 50 μg/ml (same cell as depicted in Fig. 1) or of 5 μg/ml Rh-EGF. The 5 μg/ml concentration could not be used for HER22 cells since the level of fluorescent intensities is within the background of detection of our system. The intensity at the plateau is five- to eightfold higher for HER82 cells than for the HER22 cells when 50 μg/ml of Rh-EGF is used. HER82 cells incubated with tenfold less Rh-EGF have a time course of internalized intensity similar to HER22 cells. HER82 cells incubated with the same Rh-EGF concentration but different total EGF concentrations had similar maximum internalized intensities. These cells, which were labeled with a 4-μl aliquot of one part 50 μg/ml Rh-EGF plus nine parts PBS or one part 50 μg/ml Rh-EGF plus nine parts 50 μg/ml unlabeled EGF, had six- to eightfold lower intensities than when saturating (50 μg/ml) concentrations of Rh-EGF were used (Table I). Nonspecific fluorescence, as determined with incubation of Rh-EGF and a 50-fold excess of unlabeled EGF, was under the typical threshold levels for these experiments and, thus, was removed by subtraction of the subthreshold background (see Materials and Methods). Previous measurements have also shown that the change of fluorescence intensity (nonspecific background subtracted) between HER82 and HER22 cells labeled with 50 μg/ml of Rh-EGF was directly proportional to the number of EGF-binding sites found on their cell surface (Benveniste et al., 1988).

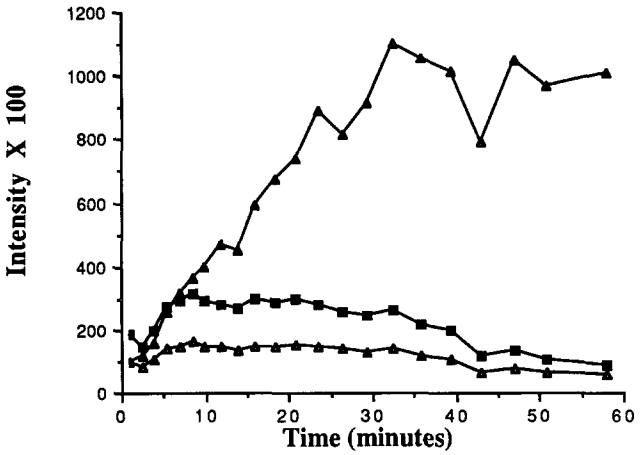

Figure 7. Effects of video-digitized intensity calibration and correction for bleaching on the time dependence of the internalized integrated intensity above threshold (=35) of an HER22 cell. (■) Original data; (△) after calibration and normalization for camera gain; (▲) after normalization for camera gain and bleach correction.

Fig. 9 shows the respective time dependence of the internalized endosome areas for the same cells from Fig. 8. The rates of increase and the absolute levels of internalized areas are similar for all cases even though the HER82 cell has on the average 7.5-fold more receptors than the HER22 cell and the total internalized EGF is different. The kinetics of the increase in internalized intensity, area, and vesicle number peak 10 min after the start of the experiment and start to decay after 30 min. The number of fluorescent vesicles varies two- to threefold between these three experiments and has no correlation with the intensity of internalized fluorescence (Fig. 10). Maximal internalized intensity, area, and vesicle number have been summarized for several cells in Table I. Due to high contrast of the deconvoluted pictures, a 10% change in threshold level is a reasonable estimate for error since it produces visually similar quality of vesicle segmentation of fluorescence patches. Such a change in threshold level results in a 30% change in area and intensity. However, the change in their ratio is <20%.

The local concentration of EGF within vesicles is determined by the intensity per unit area (pixel) of patches. This quantity, which we define as specific fluorescence, is time

Table I. Summary of Maximum Internalized Areas and Intensities of Fluorescence

Cell line*	Rh-EGF	Intensity	Area	Vesicles
	μg/ml	*arbitrary units (SD)*	*pixels (SD)*	n (SD)
HER82 (4)	50	5.9×10^5 (44.1)	9.2×10^3 (42.4)	194 (32.1)
HER82 (2)‡	5	7×10^4 (60.6)	3.3×10^3 (10.9)	130 (2)
HER22 (6)	50	2.8×10^4 (129)	3.1×10^3 (67)	182 (25.8)

Area and fluorescence intensities were summed for all pixels above threshold. The number of vesicles is the number of contiguous patches.
* Number of samples in parentheses.
‡ In one experiment, cells were incubated with a 4-μl aliquot of one part 50 μg/ml Rh-EGF plus nine parts PBS, while in the second experiment cells were incubated with a 4-μl aliquot of one part 50 μg/ml Rh-EGF plus nine parts 50 μg/ml unlabeled EGF.

dependent as shown when the average slope of a plot of intensity vs. area for fluorescent patches is determined individually for each time group. Fig. 11 shows that the specific fluorescence of the HER82 cell incubated with 50 μg/ml Rh-EGF rises approximately fourfold, reaching a plateau 50 min after the start of the experiment. The specific fluorescence of an HER82 cell incubated with 5 μg/ml Rh-EGF and an HER22 cell labeled with 50 μg/ml Rh-EGF increases about twofold.

In Fig. 12, the integrated intensities of the fluorescent patches are plotted against their respective number of pixels (area). Each point in this figure represents the average of the intensities of all patches of the same area collected from all groups of images of an HER82 cell. The specific fluorescence can be described by the slope of the two linear fits for patch areas above and below a 50-pixel area. Fig. 13 is a summary of all the data subjected to the analysis exemplified in Fig. 12. The large cell-to-cell variations in total Rh-EGF binding make it difficult to evaluate trends between the transfected cell lines. Since there is a direct correlation between Rh-EGF binding and the maximum internalized fluorescence intensity (Fig. 8 and Table I), local, internalized Rh-EGF concentrations can be normalized. Fig. 13 clearly shows that the specific fluorescence for both small and large patch areas increases linearly as the total maximum internalized intensity increases. The specific fluorescence of patches with an area >50 pixels is twofold higher than the corresponding specific fluorescence of patches <50 pixels. The x-intercept of the slope of specific fluorescence of large patches (Fig. 12, *inset*) also increases with increasing maximal internalized intensity, from 18.7 pixels for HER22 cells to 29.7 pixels for HER82 cells.

Single vesicles within a specific HER82 cell were tracked manually and analyzed. Vesicle intensities and areas (data not shown) increased with time, with the areas >50 pixels appearing after 10 min at 37°C. Table II summarizes results for the specific fluorescence obtained for five fluorescent vesicles traced within a specific cell. The average slope for the specific fluorescence for small and large vesicles was 18 and 55 grey levels per pixel, respectively, and the x-intercept was 28 pixels. This data correlated well with results obtained by the automatic thresholding technique. The vesicle coordinates exhibit a saltatory movement whose general direction approached the cell center.

Discussion

Fluorescence microscopy provides a way to localize labeled molecules and measure their concentrations in live intact cells. Fluorescent images have large out-of-focus contribu-

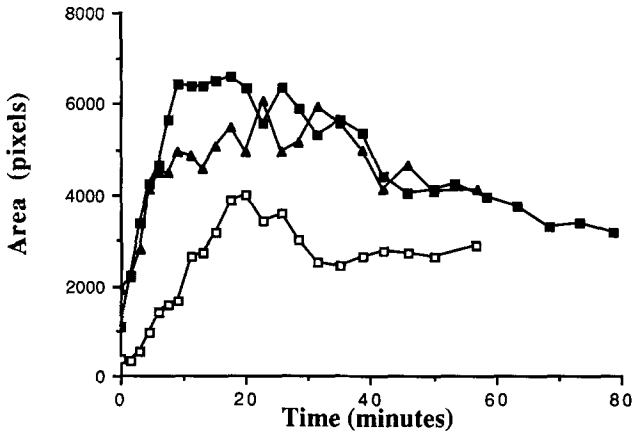

Figure 9. Time dependence of internalized fluorescent patch areas in NIH-3T3 transfected cells of Fig. 8. Internalized areas above threshold of each time group are summed and plotted for (■) HER82 cell labeled with 4 μl of 50 μg/ml Rh-EGF; (▲) HER22 cell labeled with 4 μl of 50 μg/ml Rh-EGF; and (□) HER82 cell labeled with 4 μl of 5 μg/ml Rh-EGF.

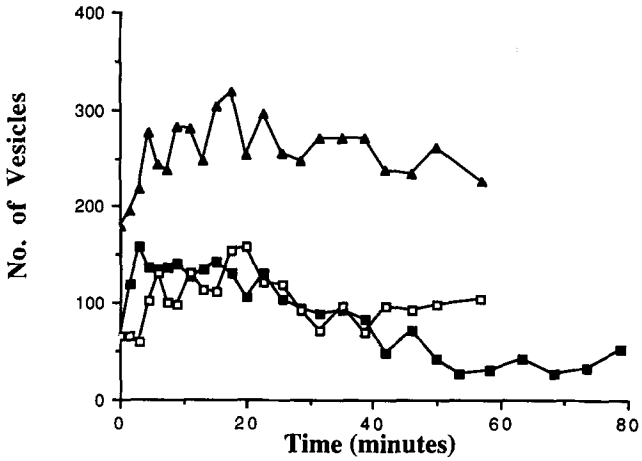

Figure 10. Time dependence of the number of internalized vesicles in the NIH-3T3 transfected cells of Fig. 8. Fluorescent patches above threshold of each group are counted for (■) HER82 cell labeled with 4 μl of 50 μg/ml Rh-EGF; (▲) HER22 cell labeled with 4 μl of 50 μg/ml Rh-EGF; and (□) HER82 cell labeled with 4 μl of 5 μg/ml Rh-EGF.

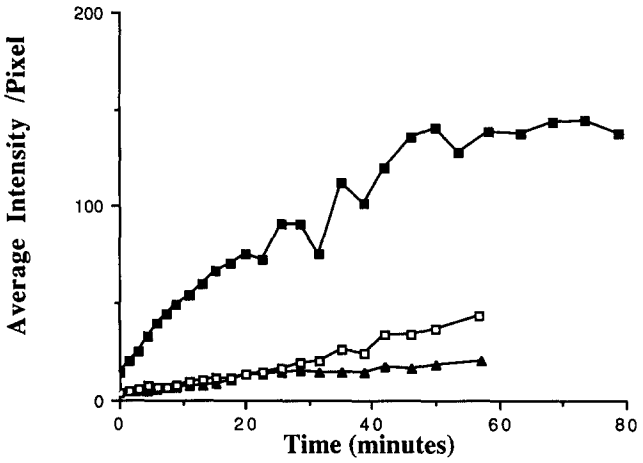

Figure 11. Time dependence of the specific fluorescence of NIH-3T3 transfected cells of Fig. 8. Slopes were determined from plots of vesicle intensities vs. vesicle areas for each time group for (■) HER82 cell labeled with 4 μl of 50 μg/ml Rh-EGF; (▲) HER22 cell labeled with 4 μl of 50 μg/ml Rh-EGF; and (□) HER82 cell labeled with 4 μl of 5 μg/ml Rh-EGF.

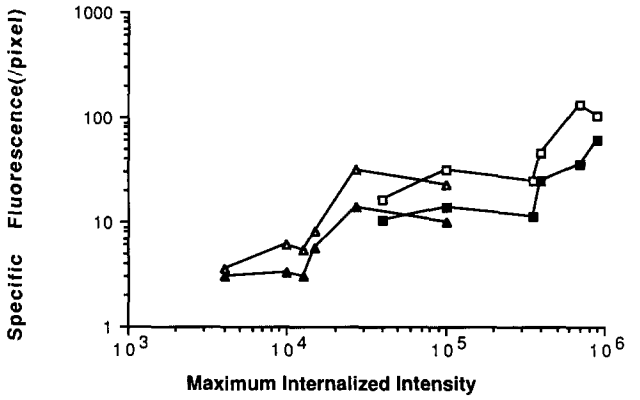

Figure 13. The dependence of specific fluorescence of transfected amplification EGF receptor cell lines on the internalized fluorescence. Slopes determined from intensity vs. area plots (Fig. 12) are drawn against the maximum internalized intensity. (■ and ▲) The specific fluorescence determined for vesicle areas <50 pixels for HER82 and HER22 cells, respectively; (□ and △) the specific fluorescence determined for vesicle areas >50 pixels.

tions (Fig. 1), which results from the fact that a point source imaged at different focal heights yields a cone of fluorescent light where the integrated intensity at any height is almost conserved, even at several microns above or below the focus (Kam, 1987). The cell contains an uneven three-dimensional distribution of fluorescent sources. Thus, each image plane contains sharp features from sources in adjacent focal planes and more diffuse features from far focal planes, contributing to a nonuniform background. Therefore, removal of low frequency contributions with a high-pass filter is not adequate to improve the contrast of the image. By using the Agard and Sedat algorithm (1980) of three-dimensional deconvolution of the microscope optical transfer function for a set of two-dimensional images at different focal heights, out-of-focus fluorescence contributions were practically eliminated. The deconvolution localizes the contribution of each vesicle to only one optical section, automatically allowing the use of simple thresholding for segmentation of endosomes (Fig. 3).

The recent popularity of scanning confocal microscopy has been warranted because of the enhanced contrast attained for fluorescent objects in real time, making deconvolution of the digitized picture unnecessary (for review see Fine et al., 1988). Signal-to-noise ratios sufficient to differentiate structure in live cells by scanning confocal microscopy have been limited to highly fluorescent lipid and intracellular dyes. Studies with more specific probes, such as fluorescent antibodies, have been limited to fixed tissues. Currently, the length of time needed to repeatedly digitize and sum optical sections by scanning confocal microscopy to acquire a signal-to-noise ratio comparable with the deconvoluted images presented in this paper is two- to threefold longer than the time required by our method. Therefore, our method of data acquisition and analysis provides better signal-to-noise ratios per unit time and an increased temporal resolution that allows

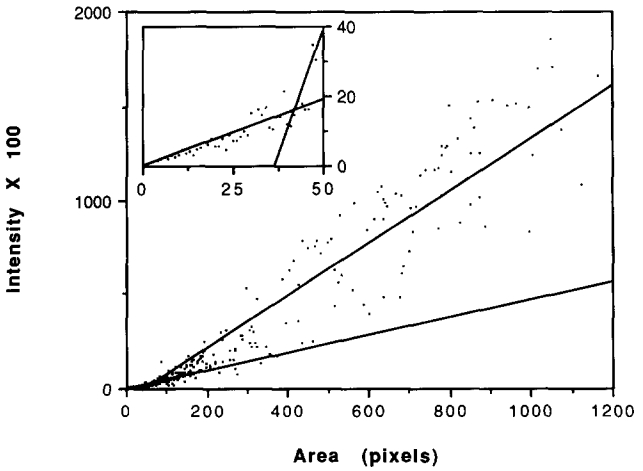

Figure 12. An example of the determination of specific fluorescence for an HER82 cell labeled with 50 μg/ml Rh-EGF. Integrated intensities (background subtracted) were summed for each patch. Intensities of all patches of the same area were averaged and plotted. A slope of 37 of the fitted line defines the specific fluorescence for patches <50 pixels and of 144 for patches >50 pixels. (*Inset*) Expanded scale for fluorescence patches <50 pixels.

Table II. Summary of the Specific Fluorescence of Individual Vesicles Manually Tracked in an HER82 Cell

	Specific fluorescence		
Vesicle	Slope 1*	Slope 2*	*x*-intercept‡
1	19.3	59.8	37
2	17.1	55.7	25
3	18.1	63.2	30
4	18.6	42.9	20
5	17.1	54.3	28
Average	18.0 ± 1.0	55.2 ± 7.7	28 ± 6.3

Slope 1 is the slope of intensity vs. area plot (Fig. 12) for patches with areas <50 pixels. Slope 2 is the slope of intensity vs. area plot (Fig. 12, *inset*) for patches with areas ≥50 pixels. *x*-intercept for slope 2 determines the extrapolated nonfluorescent area to which fluorescent vesicles fuse.
* Grey levels per pixel.
‡ Pixels.

noninvasive investigation of some biological processes in live intact cells.

Long duration exposures from the incident light source cause a decrease in fluorescence intensities due to bleaching of the fluorophore (Fig. 6). The exponential bleach decay constants, calculated from the total cell fluorescences from each experiment, show that the bleaching is only a function of the illumination conditions. The rate of bleaching of fluorescent probes was reported to depend on their environment in different cellular compartments (Benson et al., 1985). However, the total averaged cellular fluorescence decay from Rh-EGF when most of the fluorophores were bound to the membrane or localized in the endosomes, Golgi apparatus, or lysosomes was similar, suggesting that changes in fluorescence localization did not significantly affect bleaching kinetics. Thus, the bleach correction enables analysis of single cell experiments even if long exposure to fluorescent light is required. The initial rise and plateau of internalized Rh-EGF obtained for single cells by this method is similar to the kinetics of endocytosis measured with ^{125}I-EGF for plates containing millions of cells (Benveniste et al., 1988). The decrease of integrated fluorescence after the plateau sometimes detected in these curves may be due to degradation and expulsion of Rh-EGF (Carpenter and Cohen, 1976*a*).

The wide range of intensities emitted by fluorescence samples requires that the image intensifier of the video camera vary its gain to optimize the use of its dynamic range. Our data have been normalized using a calibration scale inserted into each picture to compensate for these changes of gain and allow for comparison of different data sets.

The fluorescent patches inside the cell had to consist of at least two adjacent pixels above threshold to limit the probability of counting random noise. The dimensions of a two-pixel patch, 0.14 × 0.28 μm, is ~20-fold larger than the size reported for early endosomes by electron microscopy (Hopkins, 1986). The diffuse fluorescence of early endosomes has been measured by light microscopy (Yamashiro and Maxfield, 1987), however, single vesicles were not resolved.

We have used image-intensified fluorescence microscopy in conjunction with the computer-assisted image corrections to get quantitative time-dependent observations of receptor-mediated endocytosis of EGF through coated pits. The kinetics and distribution of the process were studied at varying concentrations of the participating molecules. Transfected cell lines with amplified expression of the EGF receptor provide a way to vary the number of receptors in the plasma membrane in addition to changing EGF concentration. 5-min incubations were chosen since the amount of endocytosis occurring within that period is only 10% of the maximum total internalized fluorescence intensity. During this time, EGF binding does not reach equilibrium, yet longer incubations would prevent the observation of the kinetics of the rise in internal fluorescence. Low temperature incubations, which arrest endocytosis, were not used due to possible temperature-dependent artifacts that may change the behavior of the system (Gaskin et al., 1974; Benveniste et al., 1988).

Table I shows that HER82 cells incubated with 50 μg/ml Rh-EGF have an 8.5-fold higher average intensity than HER82 cells incubated with 10% the Rh-EGF concentration and >20-fold higher average intensity than Rh-EGF–labeled HER22 cells. The maximum internalized intensities have high standard deviations. This indicates that these cells, which belong to two specific tissue culture lines, are somewhat heterogeneous in their expression of EGF receptor on the cell surface. Fig. 13 shows that there is a 10-fold difference between the highest maximum internalized intensity of the HER82 and HER22 cells, which corresponds to the difference in number of receptors for each cell line as determined by Scatchard analysis (Benveniste et al., 1988). Internalized intensities and areas for the two cell lines are similar in kinetics, reaching a peak ~25 min after the start of the experiment (Figs. 8 and 9). This agrees with earlier results measured for populations of these two cell lines using ^{125}I-EGF (Benveniste et al., 1988). The validation of the microscopic analysis by radioactive methods opens applications to experiments on a very small number of manipulated cells. Since the rate of endocytosis of the two cell lines is similar, the maximum internalized intensity for each cell line is proportional to the amount of Rh-EGF initially bound to the membrane. The high degree of membrane labeling observed immediately after the Rh-EGF incubation (Fig. 1 *A*) indicates that the ligand is mostly internalized by receptor-mediated endocytosis rather than by fluid-phase pinocytosis.

Computerized microscopy not only allows the integration of fluorescence internalized in single cells but it also enables the quantization of localized concentrations of fluorescent labels in different subcellular sites. Specific fluorescence, which becomes a measure of local EGF concentration, increases three- to fourfold within internalized vesicles for each tenfold increase in maximum internalized intensity of Rh-EGF (Fig. 13).

The measurement of specific fluorescence allows us to discriminate between two opposing activation mechanisms for endocytosis: (*a*) global activation, where a critical concentration of occupied receptors on the cell surface stimulates an intermediary biochemical response that signals coated pits to internalize, independent of the number of receptors occupying them; and (*b*) selective activation, where the coated pits are internalized only after they are occupied by a sufficient number of receptors.

These two extreme models can be distinguished experimentally by determining the EGF concentration in endosomes as a function of the amount of EGF initially bound to the receptors in the membrane. If endocytosis occurs by global activation, the concentration of EGF in endosomes newly formed from coated pits should increase with the increasing number of occupied receptors, while the total number of endosomal vesicles should remain constant. If selective activation is the mechanism involved in endocytosis, the concentration of EGF in endosomes should be constant, while the number of endosomal vesicles should increase with the increasing number of occupied receptors. Obviously, methods measuring the total amount of endocytosed EGF cannot discriminate between the two cases.

The significant increase in specific fluorescence when EGF or its receptor concentrations are increased (Fig. 13) suggests that the global model is the probable mechanism for activation of endocytosis. The global model also is supported by the fact that the time course of internalization of fluorescent patches does not vary proportionally to either EGF or receptor concentration (Fig. 8). Furthermore, changes in vesicle number did not correlate with changes in internalized intensity (Fig. 10 and Table I). These experiments with Rh-EGF cannot determine if global activation of endocytosis is induced

by EGF ligand binding or if EGF enhances the rate of a constitutive endocytic pathway. Preliminary experiments recording endocytosis of fluorescently labeled Fab fragments with and without unlabeled EGF indicate enhancement of accumulated fluorescence in large vesicles by the EGF. However, the specific fluorescence of small vesicles was independent of the presence of EGF. This may indicate that endocytosis is constitutively activated, but EGF affects the intracellular routing and sorting of internalized membrane patches.

The critical element in differentiating between the selective trapping and global activation models is based on knowing the concentration of ligands and receptors in endosomal vesicles directly formed from internalization of coated pits. The resolution of fluorescence-computerized microscopy does not allow the observation of those endosomes, but larger vesicles, which are the product of several fusion events, can be observed. Fig. 12 shows that the relationship between small patch areas and their fluorescence intensities is linear, which is the expected result for fusion between vesicles where membrane area is conserved. The integrated intensities are measured for the whole vesicle and thus do not depend on whether the fluorophores are attached to the vesicle membrane or freely diffuse within it. The x-intercept of Fig. 12 defines the area of nonfluorescent vesicles to which fluorescent vesicles fuse. Fig. 12 also indicates that the initial slope of the specific fluorescence extrapolates to the origin. The precision of this measurement is limited to one pixel which has a 10-fold greater cross-sectional area than the smallest endosomes found in a cell. Although our data suggest that small fluorescent vesicles fuse with each other, they may also fuse with vesicles $<0.02\ \mu m^2$ which are devoid of Rh-EGF. Thus, the kinetics of endocytosis measured by fluorescence may reflect the delivery of Rh-EGF from unresolvable endosomes to those of $0.02\ \mu m^2$ instead of the kinetics of receptor trapping and internalization.

The twofold increase in the specific fluorescence of patches >30–50 pixels in both HER82 and HER22 cells (Fig. 13) indicates that the Rh-EGF is being concentrated. This can also be observed by the increase in average specific fluorescence of all patches as a function of time as presented in Fig. 11. The x-intercept of the second slope (Fig. 12) suggests that the Rh-EGF may be routed to organelles previously devoid of the fluorescent probe that had an area of ~ 25 pixels or $0.56\ \mu m^2$. This corresponds to the approximate cross-sectional area of a lysosome, which is the final destination of Rh-EGF before degradation and expulsion into the medium (Willingham and Pastan, 1985). The change in specific fluorescence at late stages of the endocytic pathway could also be explained by a breakdown in the relationship of intensity to patch area for vesicles that span more than one focal plane or by a high concentration of many unresolved small vesicles (i.e., multivesicular bodies) or highly convoluted membranes which may be found in the juxtanuclear region of the cell (Miller et al., 1986).

Examination of the deconvoluted optical sections at a high magnification and contrast, combined with hardware and software that enabled us to flip quickly and interactively between the different focal planes of the cell as well as to follow one plane back and forth in time, has allowed the tracking of isolated vesicles. Fig. 3 shows that vesicle movement is in the direction of the center of the cell. However, a significant rounding in cell shape can also be observed over this time period (Fig. 3). To gauge the change in cell shape, the center of mass was determined from the outline of the membrane boundary of the particular optical section in which the vesicle was situated. Movement of the vesicles after subtracting of the center of mass does not seem to be oriented in a particular direction but rather had a random walk nature (data not shown). Pastan and Willingham (1981) and Willingham and Pastan (1985) have tracked vesicles containing fluorescent α_2-macroglobulin and have indicated that the vesicle movement is saltatory.

A twofold difference between slopes of specific fluorescence for small and large patch areas was also observed when individual vesicles were tracked (Table II). The x-intercept for the second slope of individually tracked vesicles is approximately the same as the value determined by the automatic thresholding technique averaged on all vesicles in the cell. Thus, quantitative results can be obtained even for a single organelle in a cell.

Previously we have shown that the relative rates of internalization of ^{125}I-EGF on these transfected NIH-3T3 cells did not increase proportionally with the increase in EGF receptor concentration initially found on the membrane (Benveniste et al., 1988) and may be limited by the capacity of coated pits and their rate of internalization. Although this study shows that the rate of coated pit internalization, which is globally activated, is independent of the number of EGF receptors trapped in them, it is still not known whether trapping in coated pits is selective for occupied receptors. This can be determined by making similar measurements on cells where EGF and the receptors are labeled simultaneously by different fluorophores. However, energy transfer between fluorescein and rhodamine due to the high concentrations in vesicle membranes makes it extremely difficult to directly relate intensities to the concentrations of the labeled molecules.

We thank Etta Livneh for many fruitful interactions and Yosef Yarden for reading the manuscript.

M. Benveniste was a Levi Eschol Fellow.

Received for publication 30 January 1989 and in revised form 19 May 1989.

References

Agard, D. A., and J. W. Sedat. 1980. Three-dimensional analysis of biological specimens using image processing techniques. *Proc. Soc. Photo-Opt. Instr. Eng.* 264:110–117.

Beguinot, L., J. A. Hanover, S. Ito, N. D. Richert, M. C. Willingham, and I. Pastan. 1985. Phorbol esters induce transient internalization without degradation of unoccupied epidermal growth factor receptors. *Proc. Natl. Acad. Sci. USA.* 82:2774–2778.

Benson, D. M., J. Bryan, A. L. Plant, A. M. Gotto, Jr., and L. C. Smith. 1985. Digital imaging fluorescence microscopy: spatial heterogeneity of photobleaching rate constants in individual cells. *J. Cell Biol.* 100:1309–1323.

Benveniste, M., E. Livneh, J. Schlessinger, and Z. Kam. 1988. Overexpression of epidermal growth factor receptor in NIH-3T3 transfected cells slows its lateral diffusion and rate of endocytosis. *J. Cell Biol.* 106:1903–1909.

Bevington, P. R. 1969. Data reduction and error analysis for the physical sciences. McGraw-Hill Inc., New York. 336 pp.

Brown, M. S., R. G. W. Anderson, and J. L. Goldstein. 1983. Recycling receptors: the round-trip itinerary of migrant membrane proteins. *Cell.* 32:663–667.

Carpenter, G., and S. Cohen. 1976*a*. ^{125}I-Labeled human epidermal growth factor binding internalization, and degradation in human fibroblasts. *J. Cell Biol.* 71:159–171.

Carpenter, G., and S. Cohen. 1976*b*. Human epidermal growth factor and the proliferation of human fibroblasts. *J. Cell. Physiol.* 88:227–237.

Carpenter, G., and S. Cohen. 1979. Epidermal growth factor. *Annu. Rev. Biochem.* 48:193–216.

Das, M., and C. F. Fox. 1978. Molecular mechanism of mitogen action: processing of receptor induced by epidermal growth factor. *Proc. Natl. Acad.*

Sci. USA. 75:2644–2648.

Dautry-Varsat, A., A. Ciechanover, and H. F. Lodish. 1983. pH and the recycling of transferrin during receptor-mediated endocytosis. *Proc. Natl. Acad. Sci. USA.* 80:2258–2262.

Dickson, R. B., J. A. Hanover, M. C. Willingham, and I. Pastan. 1983. Prelysosomal divergence of transferrin and epidermal growth factor during receptor-mediated endocytosis. *Biochemistry.* 22:5667–5674.

Fine, A., W. B. Amos, R. M. Durbin, and P. A. McNaughton. 1988. Confocal microscopy: applications in neurobiology. *Trends Neurosci.* 11:346–351.

Fox, C. F., and M. Das. 1979. Internalization and processing of the EGF receptor in the induction of DNA synthesis in cultured fibroblasts: the endocytic activation hypothesis. *J. Supramol. Struc.* 10:199–214.

Gaskin, F., C. R. Cantor, and M. L. Shelanski. 1974. Turbidimetric studies of the *in vitro* assembly and disassembly of porcine neurotubules. *J. Mol. Biol.* 89:737–758.

Goldstein, J. L., R. G. W. Anderson, and M. S. Brown. 1979. Coated pits, coated vesicles, and receptor-mediated endocytosis. *Nature (Lond.).* 279: 679–685.

Gorden, P., J. L. Carpentier, S. Cohen, and L. Orci. 1978. Epidermal growth factor: morphological demonstration of binding, internalization and lysosomal association in human fibroblasts. *Proc. Natl. Acad. Sci. USA.* 75:5025–5029.

Haigler, H., J. F. Ash, S. J. Singer, and S. Cohen. 1978. Visualization by fluorescence of the binding and internalization of epidermal growth factor in human carcinoma cells A431. *Proc. Natl. Acad. Sci. USA.* 75:3317–3321.

Honegger, A. M., T. J. Dull, S. Felder, E. Van Obberghen, F. Bellot, D. Szapary, A. Schmidt, A. Ullrich, and J. Schlessinger. 1987. Point mutation at the ATP binding site of EGF-receptor abolishes protein tyrosine kinase activity and alters normal receptor cellular routing. *Cell.* 51:199–209.

Hopkins, C. R. 1986. Membrane boundaries involved in the uptake and intracellular processing of cell surface receptors. *Trends Biochem. Sci.* 11:473–477.

Kam, Z. 1987. Microscopic imaging of cells. *Q. Rev. Biophys.* 20:201–259.

Livneh, E., R. Prywes, O. Kashles, N. Reiss, I. Sasson, Y. Mory, A. Ullrich, and J. Schlessinger. 1986. Reconstitution of human epidermal growth factor receptors and its deletion mutants in cultured hamster cells. *J. Biol. Chem.* 261:12490–12497.

Miller, K., J. Beardmore, H. Kanety, J. Schlessinger, and C. R. Hopkins. 1986. Localization of epidermal growth factor (EGF) receptor within the endosome of EGF-stimulated epidermoid carcinoma (A431) cells. *J. Cell Biol.* 102:500–509.

Pastan, I. H., and M. C. Willingham. 1981. Journey to the center of the cell: role of the receptosome. *Science (Wash. DC).* 214:504–509.

Prywes, R., E. Livneh, A. Ullrich, and J. Schlessinger. 1986. Mutations in the cytoplasmic domain of EGF receptor affect EGF binding and receptor internalization. *EMBO (Eur. Mol. Biol. Organ.) J.* 5:2179–2190.

Schlessinger, J., A. B. Schreiber, A. Levi, I. Lax, T. Libermann, and Y. Yarden. 1983. Regulation of cell proliferation by epidermal growth factor. *Crit. Rev. Biochem.* 14:93–111.

Stokseth, P. A. 1969. Properties of a defocused optical system. *J. Opt. Soc. Am.* 59:1314–1321.

Willingham, M. C., and I. H. Pastan. 1982. Transit of epidermal growth factor through coated pits of the Golgi system. *J. Cell Biol.* 94:207–212.

Willingham, M. C., and I. Pastan. 1985. The pathway of endocytosis. *In* Endocytosis. M. C. Willingham and I. Pastan, editors. Plenum Publishing Corp., New York. 1–44.

Yamashiro, D. J., and F. R. Maxfield. 1987. Kinetics of endosome acidification in mutant and wild-type Chinese hamster ovary cells. *J. Cell Biol.* 106:2713–2721.